

Introduction to Strain and Texture Measurements in Polycrystalline Bulk Samples

Jon Almer and Ulrich Lienert

*Advanced Photon Source, Argonne National Laboratory, Argonne, IL 60439**

1) Introduction

This paper provides concise guidelines for an in-situ strain/texture experiment which is part of the Neutron/Synchrotron Summer School. A comprehensive description of the field is not intended.

Polycrystalline materials encompass large groups of materials such as metals, ceramics and minerals. The field of interest is the understanding of the behavior of such materials under thermo-mechanical processing, *e.g.* rolling, annealing, We concentrate here on the internal strains and stresses as well as grain orientation aspects (texture). The properties depend in many cases on the local position within the sample and may be mapped if the spatial resolution of the probe is sufficient.

The dynamical behavior at surfaces is often not representative of the bulk due to effects such as stress relaxation or abnormal grain growth. The interest here is on bulk properties which may determine quantities as diverse as mechanical strength or the critical current in superconducting tapes. Therefore a bulk penetrating probe is required such as high energy X-rays (40 to 100 keV). Third generation high energy synchrotrons like the APS provide high energy X-rays of unprecedented brilliance enabling high spatial resolution and, in combination with 2D-detectors, fast data acquisition. High energy X-rays are therefore particularly suited for *in-situ* investigations and rather complementary to neutrons which in general provide even higher penetration power but substantially coarser spatial resolution and slower data acquisition.

2) Stress and strain

Polycrystalline bodies deform when subjected to external or internal loads. The deformation is manifested in displacements of the points in the body from their initial (unloaded) positions – that is the strain. As long as the loads are small the deformation is recoverable – **elastic** strain. For large loads the material undergoes **plastic** deformation in addition to the elastic one. Diffraction techniques (neutrons and X-rays) are the method of choice for quantifying the elastic strain. With some restrictions the elastic strain is directly proportional to the stress.

2.1) Definition of stress and strain tensors in continuum mechanics

Stress: Consider a homogeneous cube subject to an external force F applied to one of its faces with cross section A , *cf.* fig. 1. Then by definition the stress σ is $\sigma = F/A$. The force can be applied along the normal to the plane (normal force) or along one of the two in-

* e-mail: almer@aps.anl.gov, lienert@aps.anl.gov

plane directions (shear force). As there are three directions (x_1, x_2, x_3) this leads to the stress tensor concept

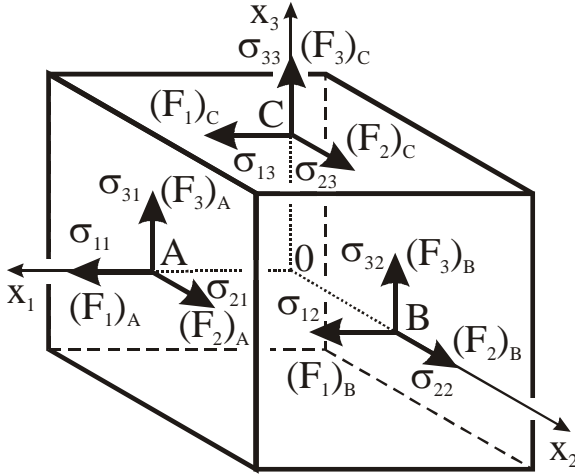


Fig. 1: The resolved forces F_i and the corresponding stresses σ_{ij} on the faces of a unit cube in static equilibrium. *cf.* Noyan and Cohen p. 16.

$$\sigma_{ij} = \begin{pmatrix} \sigma_{11} & \sigma_{12} & \sigma_{13} \\ \sigma_{21} & \sigma_{22} & \sigma_{23} \\ \sigma_{31} & \sigma_{32} & \sigma_{33} \end{pmatrix} \quad (1)$$

By convention, the second index defines the normal of the plane in which the stress acts and the first index indicates its direction. For the normal forces a positive stress indicates a tensile stress and a negative a compressive stress state. Symmetry requires the tensor to be symmetric. Stresses are measured in MPa or GPa.

Strain: Consider a line segment in a homogeneous body along the direction x , *cf.* fig. 2.

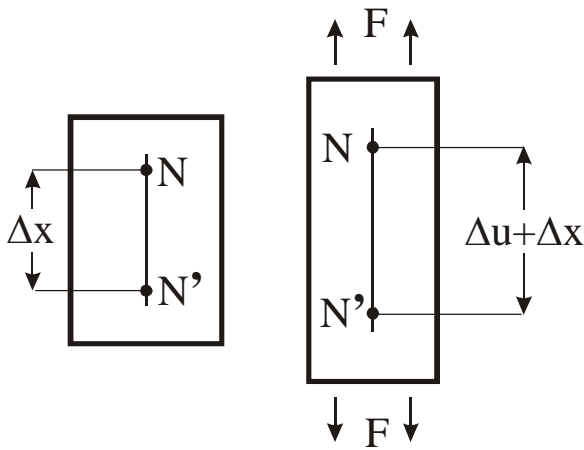


Fig. 2: Definition of the displacement Δu of a line segment of length Δx when subject to a uniform load. From Noyan and Cohen p. 17.

In the unloaded position the distance between points NN' is Δx . After subjecting a uniform load to the body the distance becomes $\Delta x + \Delta u$, where u is the displacement. The strain in the direction shown is then defined as

$$e_x = \lim(\Delta x \rightarrow 0) \frac{\Delta u}{\Delta x} = \frac{du}{dx} \quad . \quad (2)$$

Analogously to the definition of the stress tensor we can now define a tensor

$$e_{ij} = \begin{pmatrix} e_{11} & e_{12} & e_{13} \\ e_{21} & e_{22} & e_{23} \\ e_{31} & e_{32} & e_{33} \end{pmatrix} \quad (3)$$

where e_{ij} is defined as the displacement in the i direction for an initial line segment aligned with the principal direction j . However, when subject to load any rigid body will in general rotate at the same time as it distorts. In order to obtain the strain associated with distortion the rotation part must be removed. This can be accomplished by making the tensor symmetrical (see *e.g.* Noyan and Cohen). The strain tensor is then defined as

$$\varepsilon_{ij} = \begin{pmatrix} \varepsilon_{11} & \varepsilon_{12} & \varepsilon_{13} \\ \varepsilon_{21} & \varepsilon_{22} & \varepsilon_{23} \\ \varepsilon_{31} & \varepsilon_{32} & \varepsilon_{33} \end{pmatrix} = \begin{pmatrix} e_{11} & (e_{12} + e_{21})/2 & (e_{13} + e_{31})/2 \\ (e_{12} + e_{21})/2 & e_{22} & (e_{23} + e_{32})/2 \\ (e_{13} + e_{31})/2 & (e_{23} + e_{32})/2 & e_{33} \end{pmatrix} \quad (4)$$

It is instructive to distinguish between a deformation leading to shape changes – distortion – and one leading to dimensional change only, without a change in shape – dilatation. The normal strains ε_{ii} contain the dilatation part $\Delta = \varepsilon_{11} + \varepsilon_{22} + \varepsilon_{33}$. The average $\Delta/3$ is known as the hydrostatic strain. By subtracting the hydrostatic strain from the original strain tensor we get the so-called deviatoric strain tensor. Strains are dimensionless figures, often quoted in units of microstrains (multipla of 10^{-6}).

For a homogeneous material the stress tensor σ_{ij} can be derived from the strain tensor by Hooke's law

$$\sigma_{ij} = \sum_{kl} C_{ijkl} \varepsilon_{kl} \quad (5)$$

where C_{ijkl} is the compliance tensor, containing the elastic constants. C_{ijkl} is a tensor of rank 4, that is it contains $3^4 = 81$ elements. In general symmetry reduces the number of independent elements substantially, *e.g.* for cubic systems there are only 3.

3) Partitioning of stresses and strains in a polycrystalline material

Stresses and strains in polycrystalline materials are caused by externally applied loads and /or by incompatibilities of the constituent phases. Frequently different phases show different elastic and plastic behavior, thermal expansion or phase transitions. Thus, stresses and strains are often introduced during materials processing and are called residual stresses/strains if no external load is applied.

The building blocks of polycrystalline materials are grains which are considered here as small single crystallites (in reality grains are not perfect crystals but have a mosaicity which increases with deformation). Single crystals deform in general anisotropic under elastic and plastic loads. Because the grains in a polycrystalline material have in general different orientations (as described by the texture), they will deform differently under an applied load. Thus even a single phase material may consist of elastically and plastically heterogeneous units which are however constrained to form a continuous body. The microscopic strain and stress fields in polycrystalline materials are therefore discontinuous and interactions may arise between grains which are the subject of ongoing research and beyond the scope of this paper.

A modified version of equation (5) can be applied utilizing the conventional partitioning of the stresses and strains into macro- (type I) and micro-stresses/strains (type II & III), *cf.* fig. 3.

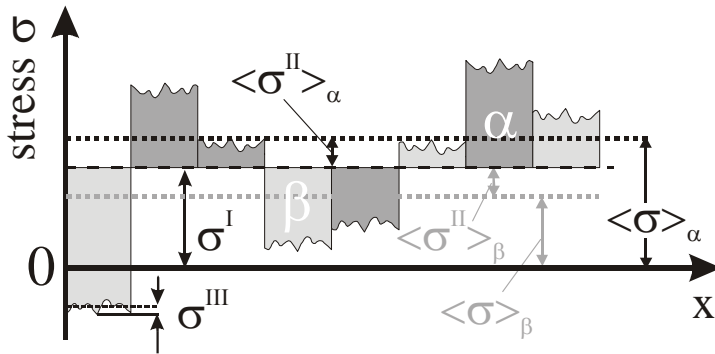


Fig. 3: Conventional stress partitioning within a two phase (α , β) material. The abscissa indicates spatial position within the sample and the histogram bars indicate the stress state in single grains. Brackets $\langle \sigma \rangle$ indicate volume averaging. From Hauk, p. 60.

Macrostress, σ^I , is defined as the volume average over a statistically representative number of grains (the averaging volume should be small compared to the length scale over which the macroscopic stress field varies). Type II stresses, $\langle \sigma^{II} \rangle_{\alpha,\beta}$, are defined as the deviation of the volume averaged phase stress from the macrostress σ^I . The sum of type II stresses over all phases is therefore zero. Note that each grain of a particular phase may have a different stress state due to the fact that the grains have different orientations and may interact with neighboring grains. Type III stresses, σ^{III} , are defined as the local variations within a single grain. Equation (5) holds for the averaged phase stresses and strains $\langle \sigma^{II} \rangle_{\alpha,\beta}$ if the elastic constants reflect the orientational distribution (texture) of the grains. For random orientation distribution, the so called quasi-isotropic case, the elastic constants have been tabulated for many materials.

For the interpretation of diffraction experiments, the elastic constants depend also on the investigated lattice planes as indexed by the Miller indices hkl . The hkl dependency

reflects the selective nature of the diffraction process and the elastic anisotropy of the crystallites (*i.e.* there are stiff and weak directions). The so-called X-ray Elastic Constants can be calculated from single crystal elastic constants assuming some model describing the crystallite coupling. Limiting cases assume that there is only dilatation but no distortion of the grains (Voigt model) and that all grains are subjected to the same stress (Reuss model). The Hill model takes the average of the Voigt and Reuss models and is found to be close to measured X-ray Elastic Constant in many cases.

4) High-energy synchrotron radiation

High-energy X-rays offer a unique tool for materials characterization, based on the following characteristics:

4.1) Penetration power

The penetration depth of high energy X-rays into several materials is presented in fig. 4. In the transmission mode, penetrations of 1-2 mm are almost universally available, while depths in the range of cm are possible for lighter materials. The penetration power in reflection mode is a factor of $\sin(2\theta)/2$ smaller than for the transmission case.

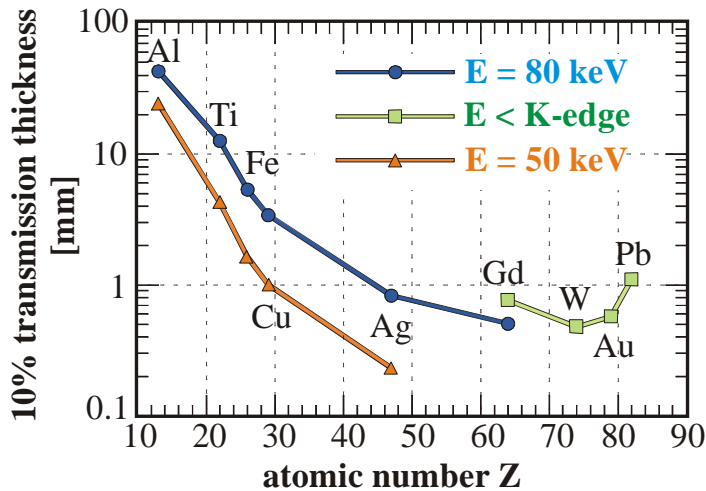


Fig. 4: Penetration power of high energy X-rays.

4.2) Small Bragg angles

Due to the short wavelengths employed, Bragg's law (see equation (6)) implies that diffraction angles for low indexed reflections ($d > 1 \text{ \AA}$) are about 5-10 degrees. This compression of the scattering to the forward direction permits access to a large q -range, simultaneously, with an area detector. From the perspective of strain measurements, at such low angles susceptibility to certain systematic errors is high. These can be mitigated by using a calibrant powder, of known d -spacing, and employing long sample-detector distances (order of m), which has the additional benefit of increasing the momentum (and

thus strain) resolution. Ideally, the detector should have a large area, in order to fulfill requirements of both large q-range and long sample-detector distances.

4.3) Spatial resolution

Recent efforts, specifically at the ESRF, have demonstrated the ability to create gage volumes with high energy X-rays on the order of $1 \times 5 \times 200 \mu\text{m}^3$, using focussing optics and conical slit assemblies. In combination with high penetration depths, such probe volumes offer truly unique abilities for depth-resolved materials studies. In practice, the minimal gage volume is often determined by the ‘continuum requirement’ that the gage volume should contain 1000-3000 diffracting grains. Such grain-averaged information will be used in these Neutron/X-ray School experiments. Below this level, methods are being developed to track diffraction spots arising from individual grains. For further information on these concepts, the reader is referred to (<http://www.risoe.dk/afm/synch/>).

4.4) Kinematical scattering

Another major advantage of high energy X-rays is that extinction and polarization terms generally associated with diffraction are negligible. For light elements this is often true also for absorption. Hence, the integrated intensity becomes directly proportional to diffracted volume and structure factors.

4.5) Strain measurements with high energy X-rays

Polycrystalline materials consist of crystalline grains which give rise to a diffracted beam when aligned suitably in respect to a monochromatic incident beam of wavelength λ . This is described by Bragg’s equation

$$2d \sin \theta = \lambda \quad . \quad (6)$$

By measuring the scattering angle θ we obtain therefore the interatomic spacing of the diffracting lattice planes d . The strain of this diffracting grain in direction of the scattering vector q (*i.e.* the projection of the strain tensor on the scattering vector) is then

$$\varepsilon_q = \frac{d - d_0}{d_0} = -\frac{2\theta - 2\theta_0}{2 \tan \theta_0} \quad (7)$$

where the last equality follows from a partial differentiation of eq. (6) which is valid as elastic strains are small. Strain should generally be measured to an accuracy of $\pm 10^{-4}$. This requires an accurate determination of the scattering angle by finding the center of the diffraction peak. In practice d is often measured by comparison to a calibration standard which eliminates most systematic errors. Note that an accurate knowledge of the strain free lattice spacing d_0 is required by eq. (7). Accurate d_0 values are often difficult to obtain and the separation of the strain into hydrostatic (d_0 dependent) and deviatoric (d_0 independent) parts is one way to deal with this problem.

Strain is a tensor and the determination of all its components requires at least measurements in six independent directions. The appropriate treatment involves three coordinate systems (crystallite-, sample-, and laboratory-systems) and the respective

transformation matrices. Here only a simplified description pertaining to the actual experiment will be given. The geometry of the experimental setup is shown in fig. 5.

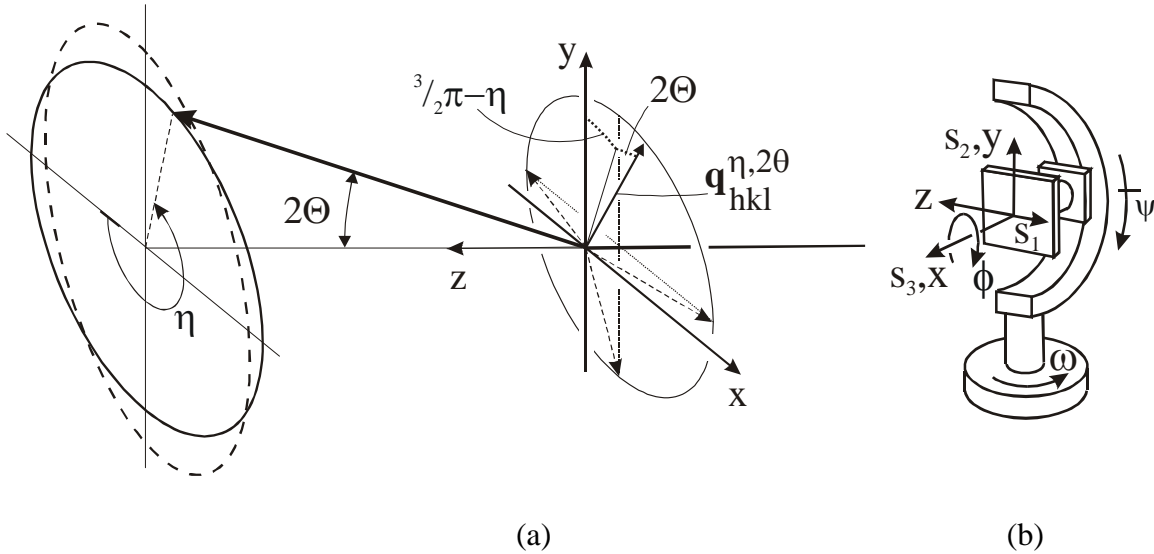


Fig. 5: (a) Scattering geometry of the experimental setup. x, y, z define the laboratory coordinate system, z being parallel to the incident beam, x is in the horizontal plane pointing outwards from the storage ring, and y is perpendicular to both z and x . The scattering vector \mathbf{q} and the diffracted beam for a diffracting grain are indicated by solid arrows. Note that all scattering vectors coinciding on a cone with large opening angle (indicated by the dashed scattering vectors) are detected simultaneously on a 2D-detector. (b) Sample coordinate system s_i . The orientation of the sample coordinate system with respect to the laboratory system is shown for $\omega = \psi = \phi = 0$.

The direction of the scattering vector in the laboratory system is given by two angles η and 2θ . Circular diffraction rings are recorded on the 2D-detector if only hydrostatic strains are present, but distorted rings result from deviatoric strains. The sample orientation in the laboratory system is defined by the three angles ω , ψ , and ϕ as shown in fig. 5b, *cf.* He *et al.*. For the present experiment the strain tensor in the sample coordinate system will be obtained by a least-square-fitting of the relative distortion of the diffraction rings (function of η and 2θ) to component equations as given by He *et al.*.

5) Texture

Texture refers to the statistical orientation of grains (or sub-grains) in a polycrystalline sample.

5.1) Coordinate systems

Crystallite system: This system describes the symmetry of the individual crystallites. For cubic symmetry, the [100], [010], and [001] directions are chosen.

Sample system: This system is fixed to the sample. In metallurgical applications, the sample system is defined by the rolling direction (RD), the transverse direction (TD), and the normal direction (ND).

“Omega” system: This system is particular to the actual experimental setup. It is fixed to the ω -rotation table. At $\omega = 0$ deg, RD is parallel to the beam, TD is perpendicular to the beam and in the horizontal plane, and ND points up.

Laboratory system: This system is fixed to the incoming beam. The convention used by polefigure.m is: x is parallel to the beam, y is perpendicular to the beam and in the horizontal plane, and z points up (note that the “standard” APS definition is different).

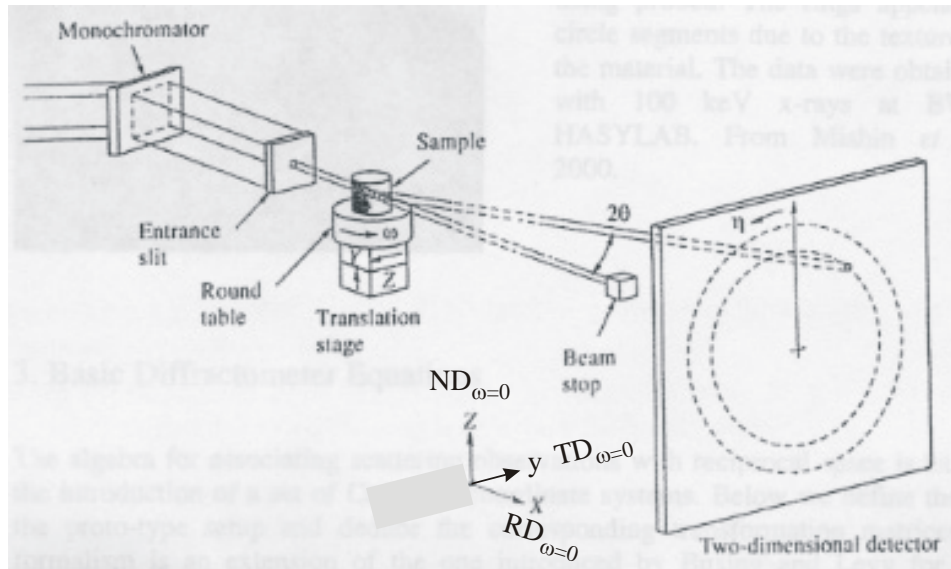


Fig. 6: Definition of the coordinate systems and rotation axes. Laboratory system (x,y,z).

The sample system (RD,TD,ND) is shown for $\omega = 0$ and $S = \begin{pmatrix} 1 & 0 & 0 \\ 0 & 1 & 0 \\ 0 & 0 & 1 \end{pmatrix}$. S represents the

transformation from the sample to the ω -system: $G_\omega = S G_S$.

5.2) Euler angles and ODF

The crystallographic orientation of a given grain or subgrain can be defined by 3 parameters. The most common representation of the 3-dimensional “orientation space” is by Euler angles (Fig. 7).

The Orientation Distribution Function (ODF) gives the density (probability) to find grains oriented with a particular orientation (as defined by the 3 Euler angles).

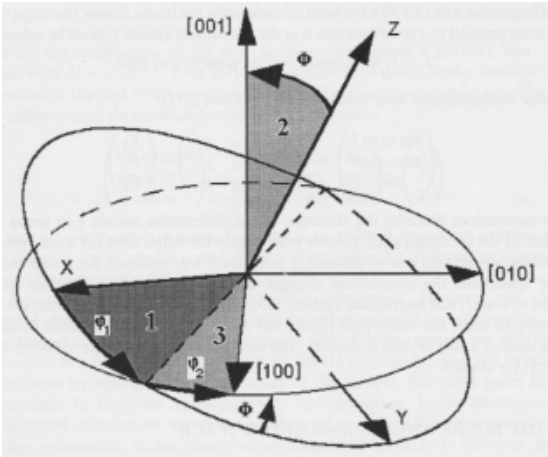


Fig. 7: Definition of the Euler angles describing the rotation between the crystallite and sample coordinate systems. (from Randle & Engler)

5.3) Polefigures

Polefigures are a 2-dimensional representation of the 3-dimensional orientation of crystallites in a sample.

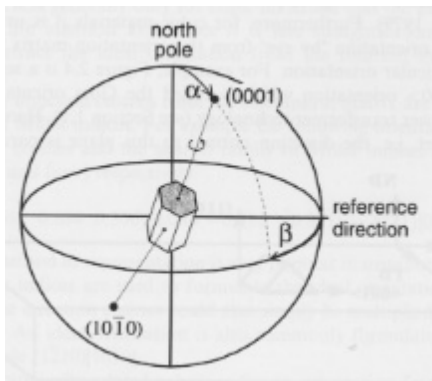


Fig. 8: Representation of the crystallite orientation by two angles α and β . Note that the rotation around the pole-axis is not defined. (from Randle & Engler)

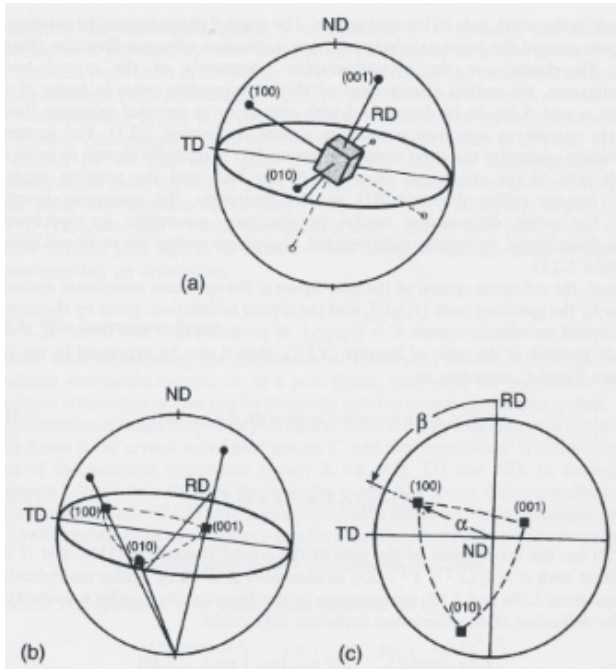


Fig. 9: Presentation of the {100} poles of a cubic crystal in the stereographic projection. (from Randle & Engler)

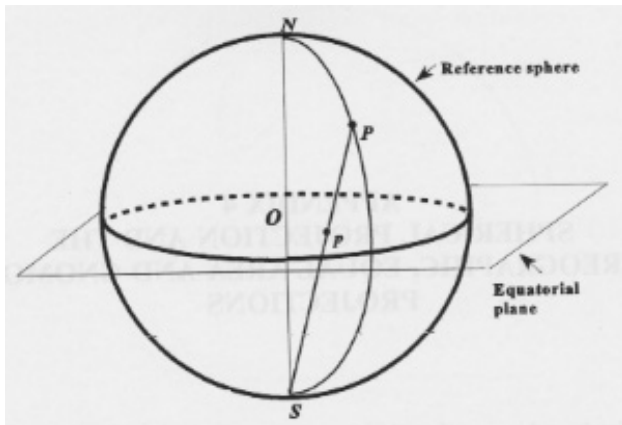


Fig. 10: Stereographical projection. (from Randle & Engler)

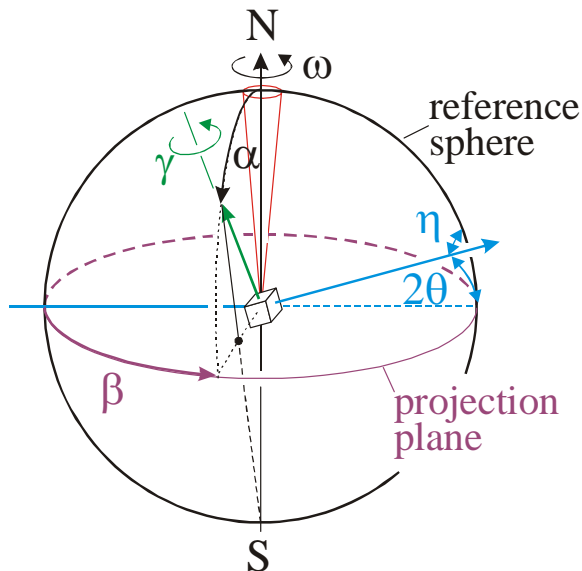


Fig. 11: Polefigure measurement with high energy X-rays.

6) Material under investigation: Duplex steel

Duplex stainless steels, consisting of approximately equal amounts of ferrite and austenite, often combine the best features of austenitic and ferritic stainless steels and are established as products ranging from heat exchangers and paper machines to chemical tankers and pressure vessels and pipes. In most cases duplex steels are selected because they combine high strength and corrosion resistance. The growing use of such steels has increased demand for understanding their mechanical behavior.

In a two-phase material like duplex stainless steel, the microstructure is inhomogeneous, and each phase will have a different response to an applied strain. Since the constituent phases have different coefficients of thermal expansion, thermal residual stresses are formed during cooling from processing temperatures. Differential elastic and plastic responses will lead to additional phase stresses during loading. Monitoring the combined effects of residual and applied strains on the deformation response is a primary goal of these experiments.

The microstructure of the duplex steel being measured is shown in fig. 12(a). The material was first hot rolled at 1050 C, and then quenched to avoid precipitation of secondary phases (this can be confirmed from phase analysis with your XRD measurements), and finally cold-rolled to 1.5 mm thickness. The microstructure is heavily banded as a result of the hot rolling, with austenitic islands existing in a ferrite matrix. The grain sizes are on the order of ten microns, and grains exhibit some preferred orientation (this can also be verified in your measurements, by non-uniform intensities around the diffraction rings). The volume fractions, determined from point counting, are 55 +/- 5% ferrite and 45 +/- 5% austenite. Due to the microstructural anisotropy, the mechanical properties vary in different directions. For details of these and other mechanical properties, and results of laboratory x-ray stress measurements of surface layers, see the attached reference by Johansson *et al.*.

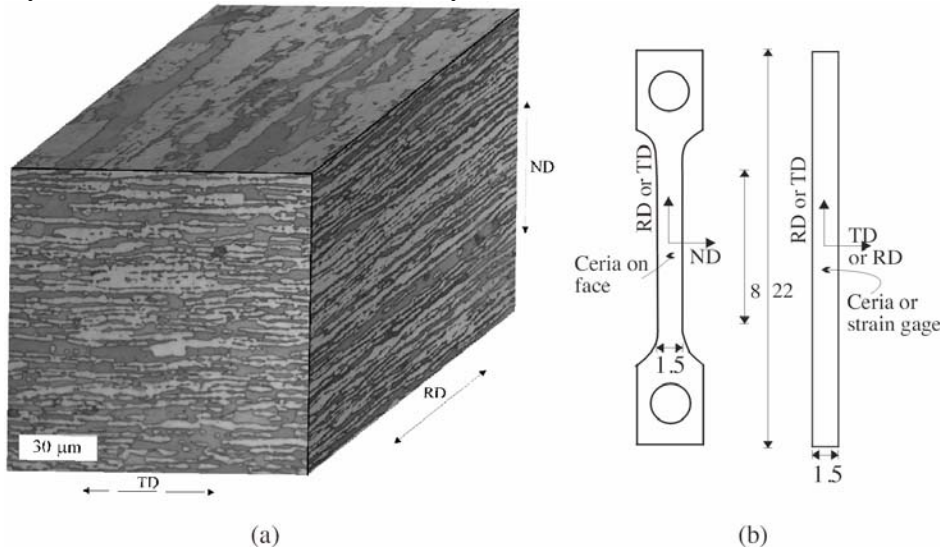


Fig. 12: Duplex microstructure and sample geometry (dimensions in mm). RD= rolling direction, ND=normal direction to rolling axis and TD= transverse direction.

The sample geometry for our experiments is shown in fig. 12(b). Electro-discharge machining was used for sample cutting, to minimize damage of machined layers, and dimensions were chosen to comply with ASTM standards for tensile testing. One sample is cut such that the loading direction (LD) is along the transverse direction, and for the remaining samples LD is along the rolling direction.

7.) References

I.C. Noyan and J.B. Cohen, 'Residual Stress', Springer Verlag, Berlin, 1986.

V. Hauk (editor), 'Structural and Residual Stress Analysis by Nondestructive Methods', Elsevier Science B.V., Amsterdam, 1997.

He B.B., Smith K.L., Proc.SEM Conf., Houston (Texas), 1998, pp. 217-220

J. Johansson, M. Oden, and X.-H. Zeng, 'Evolution of the Residual Stress State in a Duplex Stainless Steel During Loading', Acta mater. **47**, 1999, pp. 2669-2684

V. Randle, O. Engler, 'Introduction to Texture Analysis', 2000